Photofragmentation of $I_2^- \cdot Ar_n$ clusters: Observation of metastable isomeric ionic fragments

Vasil Vorsa, Paul J. Campagnola,[a] Sreela Nandi, Mats Larsson,[b] and W. C. Lineberger
Department of Chemistry and Biochemistry and JILA, University of Colorado and National Institute of Standards and Technology, Boulder, Colorado 80309-0440

(Received 6 February 1996; accepted 24 April 1996)

We report the 790 nm photofragmentation of mass-selected $I_2^- \cdot Ar_n$ clusters, $n=1$ to 27. We determine the $I^- + I$ caging efficiency as a function of the number of solvent Ar atoms and compare these results with I_2^- in CO_2 clusters. Caging is much less effective with Ar. In addition to ''normal'' caged photoproducts ($I_2^- \cdot Ar_m$, where $m<n$), the evaporation process following photoexcitation produces ''solvent-separated'' $(I^- \cdots I) \cdot Ar_m$ photofragments, where the I_2^- bond has not reformed. These metastable species comprise ~55% of the photofragment yield for precursor clusters for $n \geqslant 14$ and have lifetimes >5 μs. This unusual photofragment exists either as a trapped excited electronic state or as a solvent-separated pair at an internuclear separation of ~5.5 Å. The photofragmentation data also exhibit the existence of two distinct isomeric forms of the precursor $I_2^- \cdot Ar_n$, for $n \leqslant 14$. These forms are evaporatively distinct in that one isomer displays highly nonstatistical fragmentation, probably arising from a cluster in which the I_2^- resides on the surface, rather than in the interior. The photofragmentation distribution of the other form exhibits statistical behavior, consistent with the evaporation of an I_2^- solvated inside the cluster. © *1996 American Institute of Physics.* [S0021-9606(96)00829-X]

I. INTRODUCTION

The influence of solvents on bond formation and dissociation has received a great amount of attention in cluster studies. Examples include the caging dynamics of I_2^- in CO_2 clusters[1–3] and I_2 in Ar clusters,[4–9] where the primary goal has been to understand the detailed role of the solvent in inducing recombination of the chromophore following photodissociation. A particular aim has been to address questions regarding the efficiency of the solvent to induce geminate recombination as a function of cluster size and composition as well as the details of energy flow between the solute and the solvent. For *neutral* chromophores, although electrostatic forces play a role, the recombination and subsequent relaxation dynamics are often governed by the solvent/solute kinematics. Conversely, for an *ionic* chromophore the Coulomb interactions between the solute and solvent may be expected to dominate the reaction dynamics. Ions, with associated solvent molecules, e.g., $I_2^- \cdot (CO_2)_n$, provide a unique opportunity to investigate the role of the solvent, as incorporation of a mass spectrometer affords the selection of an ionic chromophore with a specific solvent size and composition, as has been shown in several systems.[10–18]

In this work, we examine the caging of I_2^- in a nonpolar cluster solvent (i.e., Ar). We report the photofragmentation of I_2^- in size-selected Ar clusters in which the number of Ar solvent atoms varies from 1 to 27. This range covers the generally expected size range of the first Ar solvent shell (16–25 Ar solvents). We report the effectiveness of the Ar solvent to cage photodissociated I_2^- and compare these results with the previous results[19] of a similar-mass solvent, CO_2. However, the electrostatic forces differ considerably since only shorter-range ion-induced forces are operative in the $I_2^- \cdot Ar_n$ clusters. In addition to caged and uncaged photoproducts, we find a long-lived (>5 μs) metastable photofragment ion in which the I^- and I have not recombined, but still remain within the cluster. This metastable product is present with as few as two Ar atoms composing the remainder of the cluster. This result might arise from a trapped excited state or, more likely, from a ''solvent-separated'' reactant pair, a product often observed in the condensed phase in the form of cation–anion pairs. The nonpolar nature of clusters containing rare gas atoms has been the motivation behind this study as well as a wide range of other Ar[18,20–47] and rare gas cluster studies.[48–51]

We also observe two isomeric forms of cluster ions formed in the source. In addition to the isomer that leads to the products mentioned above, a second isomer is observed that leads to a highly nonstatistical distribution of photofragments. The most likely structure of this isomer consists of an I_2^- residing on the surface of the Ar cluster, rather than in the interior. This higher-energy surface isomer is only observed in clusters with 14 or fewer Ar atoms.

In the remainder of this paper, we review cluster ion evaporation theory followed by a discussion of the dependence of binding energy as a function of cluster size. In the experimental section we present the salient features of the cluster ion source, tandem time-of-flight mass spectrometer, and laser system. Results are presented next, followed by a discussion section and conclusions.

II. REVIEW OF CLUSTER ION EVAPORATION

Studying the caging process in ionic clusters rather than in a liquid medium presents both different challenges and

[a]Permanent address: University of Connecticut Health Center, Center for Biomedical Imaging Technology, CBIT-MC 1507, Farmington, CT 06030.
[b]Permanent address: Department of Physics, Royal Institute of Technology, S-100 44 Stockholm, Sweden.

 0021-9606/96/105(6)/2298/11/$10.00

provides additional richness. Many liquid-phase experiments rely on direct changes in optical absorption to determine the state of the chromophore and thus probe caging. When studying mass-selected ionic clusters, the sample densities are far too low for this detection method. Consequently, absorber excitation and the ensuing dynamics must be determined by analysis of the cluster ion mass loss following photoexcitation of the solute chromophore. The uniqueness of cluster studies lies in the ability to monitor directly the energy transfer from the photoexcited chromophore to the solvent, which is manifest as solvent evaporation. This enables us to estimate the binding energies of the solvent to the solute, as well as to identify the various product channels.

We briefly review the relevant aspects of unimolecular decomposition of ionic cluster ensembles with a specified amount of internal energy. What follows is an overview of the salient features of statistical evaporation theory as elaborated by Klots[52,53] and Engelking.[54,55] Most cluster ion photofragmentation dynamics studies have been interpreted in terms of the evaporative ensemble model first presented by Klots in 1985.[52] In this formalism, the cluster ions comprising the ensemble are assumed to be composed of a core ion and a number n of solvent atoms each bound to the core by the same energy, ΔE_a. The energy distribution of the members of the ensemble is assumed to be Gaussian with mean total energy E and a FWHM of ΔE_a (one monomer binding energy). The rate of solvent evaporation (energy loss) from the cluster is then calculated as a function of E, ΔE_a, and cluster size n. This model can also be readily recast in terms of a cluster ''temperature'' T, ΔE_a, and n. In the experiments involving cluster ions, one generally knows the binding energy ΔE_a, the number of solvent molecules remaining on the ion after evaporation, and the length of time of evaporation. In our experiment, this time (typically between 50 and 100 μs) represents how long the cluster ion spends in the field-free region of the primary time-of-flight mass spectrometer. This model is thus used to provide an estimate of the cluster ion temperature as was, e.g., done for $(H_2O)_n^-$ clusters.[56]

Although derived from different approaches, the modified RRK theories of Klots[53] and Engelking[54] yield more or less the same rate at typical experimental energies. For simplicity, Klots' formalism will be used throughout the remainder of this paper. Klots has proposed[53] a general Arrhenius-type equation composed of preexponential, entropy, and Boltzmann terms for the unimolecular decay rate $K(T)$ of a cluster composed of n atoms as a function of temperature:

$$K(T) = An^{2/3} \exp\left(\frac{6}{n^{1/3}}\right) \exp\left(\frac{-\Delta E_a}{k_B T}\right). \tag{1}$$

Here A is the preexponential factor, terms containing n account for the entropy of evaporation, ΔE_a is the monomer binding energy, and k_B is the Boltzmann constant. The microcanonical formalism is often convenient in describing a cluster ion ensemble; for Ar this rate can be transposed into a function of internal cluster energy $K(E)$ by using the relationship

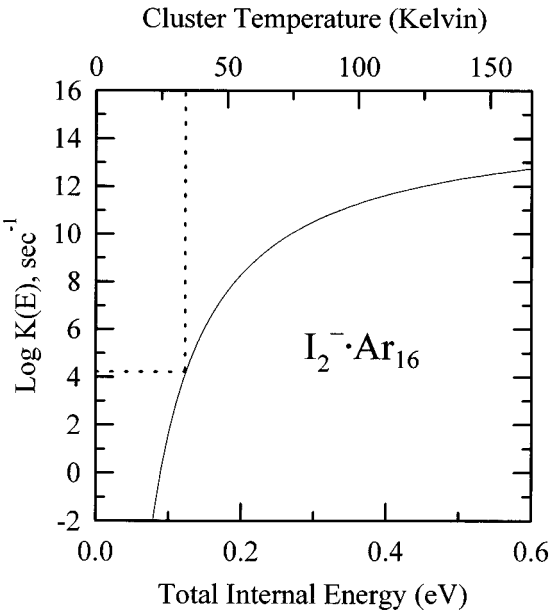

FIG. 1. Log of unimolecular decay rate $[K(E)]$ versus total internal energy (bottom x axis) and temperature (top x axis) for $I_2^- \cdot Ar_{16}$.

$$E = (3n-6)k_B T, \tag{2}$$

to yield

$$K(E) = An^{2/3} \exp\left(\frac{6}{n^{1/3}}\right) \exp\left(\frac{-\Delta E_a (3n-6)}{E}\right). \tag{3}$$

From the present photofragmentation results, the Ar monomer binding energy was calculated to be about 73 meV (Results section). This value, along with an A factor[53] for Ar of 1.3×10^{13}, yields the $\log K(E)$ versus total internal energy curve for $I_2^- \cdot Ar_{16}$ shown in Fig. 1. Cluster ion temperature is given on the top x axis. The dashed horizontal line represents the time available in our experiment (τ_1) for the evaporation of $I_2^- \cdot Ar_{16}$. The vertical dashed line gives an estimate of the $I_2^- \cdot Ar_{16}$ cluster temperature ($\sim$35 K). A more sophisticated metastable decay analysis is presented in the results section and yields a temperature of $\sim$40 K.

Following photoabsorption, the time available for solvent evaporation is $\sim$5 μs (τ_2). This is set by the distance between the laser interaction region and the entrance to the reflection mass spectrometer. Due to the logarithmic relationship between rate and energy, the photoproduct temperature upon entering the reflectron, for mass analysis, will be close to the precursor cluster ion temperature, provided that there are a sufficient number of solvent monomers remaining on the cluster.

III. BINDING-ENERGY DEPENDENCE OF CLUSTER ION SIZE

To apply accurately the above statistical theory, the monomer binding energy, ΔE_a, must be well known; the rate is exponentially dependent on this value. We estimate ΔE_a using the following equation:

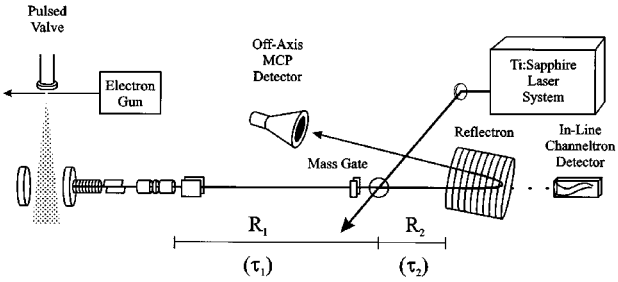

FIG. 2. Schematic diagram of the cluster ion source and tandem TOF mass spectrometer. The reflectron field can be adjusted to refocus either the precursor ions or photofragment ions of a selected mass at the off-axis microchannel plate detector. R_1 and R_2 are the primary and secondary field-free flight distances, respectively, and τ_1 and τ_2 are the respective flight times.

$$\Delta E_a \leqslant \frac{h\nu}{n_{\text{evap}}}, \tag{4}$$

where n_{evap}=the average number of solvent monomers evaporated. Past experience indicates that this estimate is relatively independent of initial cluster size, provided that the number of solvent molecules remaining on the ion after evaporation is $\geqslant 2$. Additionally, this method provides a reasonably good estimate, but some care must be taken in the interpretation, since the equality holds only in the limit of zero kinetic energy release. The kinetic theories described above suggest that the total kinetic-energy release accounts for about 10%–20% of the available energy.[52,55] In order for the calculated monomer binding energy to be valid, the cluster must be large enough to dissipate all the energy initially deposited into the chromophore through evaporation. Otherwise if the cluster is too small, complete solvent evaporation will occur before all of the photon energy is consumed, thus leaving behind a hot solute ion.

Both the ion–solvent attraction and the solvent–solvent attraction contribute to the monomer binding energy. Solvent–solvent attractions are dominant in larger clusters since the first solvent shell partially screens the ionic charge. Except for very small clusters, the combination of these two effects results in a binding energy nearly independent of clusters size.[56–59] Experimentally determined binding energies are often consistent with the reported bulk heats of sublimation or vaporization of the compound.[22,56,59,60] In this work we obtain an upper bound of 73 meV (1.7 kcal/mole) for $I_2^- \cdot Ar_n$, $n > 20$, which comes close to the ΔH_{sub} for solid Ar, 1.8 kcal/mole.

IV. EXPERIMENT

The photofragmentation experiments described here were carried out by incorporating a tandem time-of-flight (TOF) mass spectrometer with a Ti:Sapphire laser system. The details of the mass spectrometer have been described in detail previously,[1,19,61] and only the salient details will be given here. A schematic diagram of the instrument is shown in Fig. 2. The $I_2^- \cdot Ar_n$ clusters are prepared by co-expanding 300 K iodine vapor with ~3 atm of Ar in a pulsed supersonic expansion (General Valve Series 9, 0.8 mm diam orifice). A 1 keV cw electron beam ionizes the expansion just below the nozzle, and I_2^- ions are formed via attachment of slow secondary electrons. Clusters grow by the nucleation of Ar atoms around the I_2^- while drifting with the carrier gas in a field-free region. About 15 cm below the valve a pulsed, transverse, electric field extracts a small portion of the ions into a Wiley–McLaren TOF mass spectrometer. The ions are accelerated to 3 keV and brought to a temporal and spatial focus ~1.8 m downstream; the ion flight times (for the field-free region) range from ~50 μs for I_2^- to ~105 μs for $I_2^- \cdot Ar_{25}$. A pulsed mass gate located just before this focus transmits only the precursor ion of interest, thus greatly reducing background ion noise. At the spatial focus, the selected cluster ions are intersected by the laser, and the precursor and fragment ions drift in a field-free region for ~5 μs before entering a single-field reflectron mass spectrometer.[62] The reflectron, tilted at a small angle (4°), reverses the trajectory of the ions, thus separating the precursors and fragments according to their mass. The ions are detected by a dual microchannel plate detector at the spatial focus of the reflectron TOF. Precursor ion signals for normalization are simultaneously measured by the in-line channeltron detector directly behind the reflectron. Shown in Fig. 2 are the primary and secondary field-free flight regions, R_1 and R_2. For m/e of 750, the flight times (τ_1 and τ_2) through R_1 and R_2 are typically ~80 and ~8 μs, respectively.

The laser system used in these experiments is a commercial, regeneratively amplified Ti:Sapphire laser system. First, a Ti:Sapphire oscillator (Coherent Mira Basic), pumped by a 6 W Ar ion laser (Coherent Innova 90), produces a 790 nm, 80 MHz, 5 nJ pulse train with ~110 fs pulse duration. These pulses are then stretched to a few hundred picoseconds (Quantronix 4800 Series Stretcher & Compressor), sent into a Nd:YLF pumped, regenerative amplifier (Quantronix 4800 Series Ti:Sapphire RGA) and subsequently compressed back to near the original width. The final output of the laser system consists of near-transform-limited 1.0 mJ pulses with a duration of ~150 fs. The repetition rate of the ion-beam system is set to 80 Hz as a result of ion source pumping speed limitations. Precise temporal overlap of the ions with the laser is accomplished through the use of a delay generator (Stanford DG 535). The laser spot diameter at the ion beam–laser interaction region was ~4 mm.

The experimental procedure for obtaining photofragmentation spectra is as follows. The precursor ion of interest is selected with the primary time of flight and then photoexcited. Following photoexcitation, each ionic photofragment is examined by varying the electrostatic potential on the reflectron to refocus the cluster of interest. The refocus condition sends the selected ion on a specific trajectory that provides a common depth of penetration into the reflectron and a temporal focus of the ions at the off-axis detector. Each ionic fragment is separately refocused onto the microchannel plate detector and averaged between 500 and 3000 laser shots. The intensities of the photofragments are then subsequently integrated.

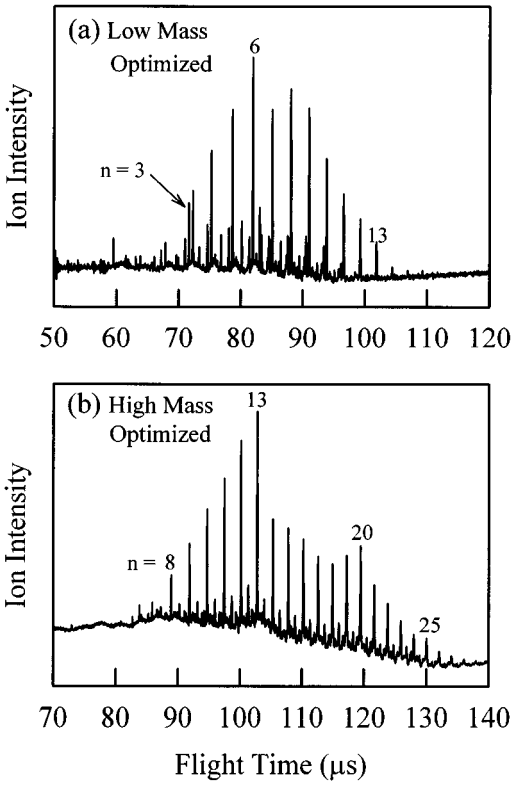

FIG. 3. Mass spectra of the precursor $I_2^- \cdot Ar_n$ cluster ions. Cluster ion source conditions are optimized for the production of (a) lower mass clusters and (b) larger mass clusters.

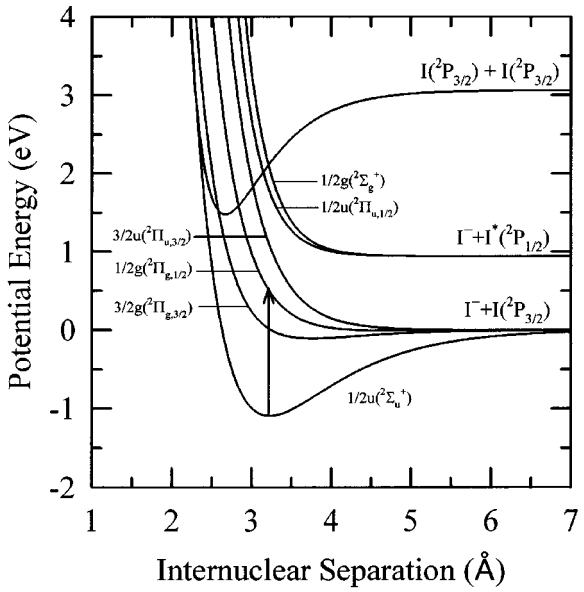

FIG. 4. Semiempirical I_2^- potential curves deduced by Chen and Wentworth (Ref. 63). Each electronic state is identified with the Hund's case (c) symmetry label. The term symbol in parentheses is the symmetry of the corresponding case (a) electronic state. The arrow indicates the $^2\Pi_{g,1/2} \leftarrow {}^2\Sigma_u^+$ near-infrared transition excited by a 790 nm photon. The ground-state potential energy curve for I_2 is included for comparison.

V. RESULTS

A. Precursor $I_2^- \cdot Ar_n$ mass spectrum and cluster ion temperature

Figure 3 shows the $I_2^- \cdot Ar_n$ mass spectrum under two sets of ion-source conditions. The position of the electron beam and the timing of the extraction pulse have been varied to optimize different regions of the mass spectrum. Figure 3(b) exhibits three regions of the mass spectrum with intensity discontinuities. The first occurs between cluster sizes $n=13$ and 14, the second at $n=20$, and the third at $n=25$. These discontinuities have been persistent throughout these experiments and do not change with different ion-source conditions.

To estimate the internal temperature of the precursor ions, we follow the method of Johnson and co-workers[56] by combining the experimentally observed metastable decay rate with the unimolecular rate theory developed by Klots[53] (discussed previously). One begins by measuring the peak intensity of a precursor ion, $I_2^- \cdot Ar_n$. Accompanying this ion in the field-free region are ions of lower mass (e.g., $I_2^- \cdot Ar_{n-1}$) arising from decay of the precursor ion and thus traveling in the same packet as the $I_2^- \cdot Ar_n$ precursor. The energy difference between the precursor and the decay products allows the reflectron energy analyzer to separate these ions in time, enabling intensity measurements to be made on both the precursor and the fragment ions. We have obtained mass spectra for the precursor ions $I_2^- \cdot Ar_{13}$ and $I_2^- \cdot Ar_{16}$ and their metastable decay products. The measured decay into the $n-1$ channel were ~7% and ~8%, respectively. Ions arising from the loss of more than one Ar atom were not detected.

Using the percentage of metastable decay products, the rate k can then be extracted from the simple first-order expression,

$$\ln \frac{C}{C_0} = -kt, \tag{5}$$

where C is the intensity of the metastable decay product, C_0 is the sum of the intensities of the metastable decay product and precursor, and t is the total field-free flight time $(\tau_1+\tau_2)$ and is on the order of 70 μs for the two products measured above. By using Eq. (1), this rate is then inverted to a temperature, providing an internal temperature of ~40 K for both $I_2^- \cdot Ar_{13}$ and $I_2^- \cdot Ar_{16}$. Since the internal energy of these clusters scales nearly linearly with size, this temperature is representative of the entire cluster ion distribution reported here except for the smaller clusters (where $n<5$).

B. Photofragment distributions for $I_2^- \cdot Ar_n$ clusters at 790 nm

All photodissociation results reported here were obtained with 790 nm wavelength laser light. At this wavelength the I_2^- is excited from its ground-state potential ($^2\Sigma_u^+$) to a repulsive ($^2\Pi_{g,1/2}$) excited state, as shown in Fig. 4.[63] Atomic Ar and neutral Ar clusters are transparent in this region of the spectrum, with the first electronic absorptions occurring in the vacuum ultraviolet.[20] Through kinetic-energy release

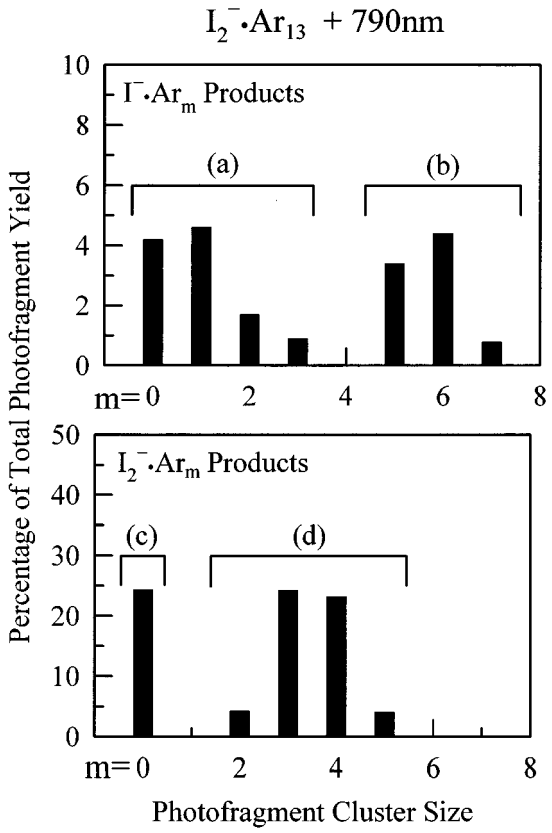

FIG. 5. Histogram of the ionic photofragments from $I_2^-\cdot Ar_{13}$ after absorption of a 790 nm photon. Indicated by brackets are the four classes of photofragments observed. The upper graph exhibits m/e 127-based (uncaged) photofragments, while the lower graph displays all the m/e 254-based photofragments (both I atoms are in the cluster).

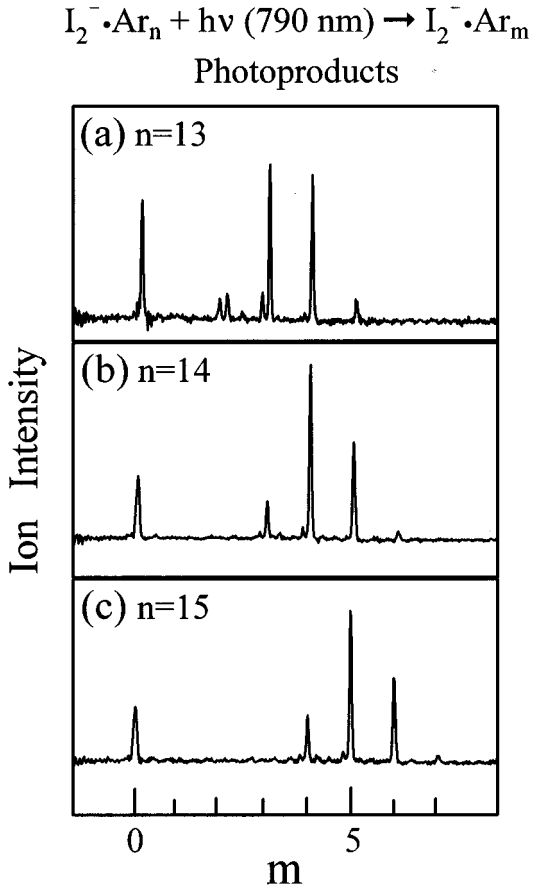

FIG. 6. Photofragment mass spectra for $I_2^-\cdot Ar_n$ after absorption of a 790 nm photon. (a) $n=13$, (b) $n=14$, and (c) $n=15$. This plot exhibits the two classes of m/e 254-based photoproducts. The average separation between the two distributions increases to ~12 Ar atoms as the precursor cluster size reaches $n=\sim 20$, at which point it remains constant. The smaller peaks to the left of peaks 2 and 3 in (a) are uncaged photoproducts.

measurements, Nadal *et al.*[64,65] have measured the bond dissociation energy to be 1.1 eV, resulting in a kinetic energy release of ~0.45 eV at this wavelength. We observe four classes of photoproducts arising from the photoexcitation of $I_2^-\cdot Ar_n$ clusters at 790 nm. For now, it will be convenient to focus our attention on $I_2^-\cdot Ar_{13}$, since it photodissociates into all four classes. A histogram of the photoproducts arising from this cluster is shown in Fig. 5, and the reaction pathways are schematically shown below:

$$\text{(a)}\quad I_2^-\cdot Ar_{13}+790\ \text{nm}\rightarrow I^-\cdot Ar_m \quad (m=0,1,2,3),$$

$$\text{(b)}\quad \rightarrow I^-\cdot Ar_m \quad (m=5,6,7),$$

$$\text{(c)}\quad \rightarrow I_2^-\cdot Ar_m \quad (m=0),$$

$$\text{(d)}\quad \rightarrow (I\cdots I)^-\cdot Ar_m \quad (m=3,4,5,6).$$

When not stated specifically, $m<n$. Channels (a) and (b) each contain clusters with only one I atom (uncaged photoproducts), but have differing amounts of Ar atoms. The average number of Ar atoms composing clusters from channel (a) is ~1, whereas the average number is ~6 for channel (b). These two distributions are clearly observed for cluster sizes between $n=10$ and 14. Channel (a) is not observed for precursors larger than $n=14$. On the other hand, for precursors smaller than $n=10$, the distributions merge together, making them indistinguishable.

The two uncaged classes also display different behavior as a function of initial precursor cluster size. The average number of Ar atoms in the photoproducts of channel (b), after evaporation, scales linearly with precursor cluster size (for $n>6$). However, channel (a) photoproducts do not scale with precursor cluster size. The average number of Ar atoms in these photoproducts is ~1, regardless of the precursor size.

Clusters in the second and third groups, (c) and (d), each contain two I atoms and therefore have m/e values based on 254 amu. The distributions are separated by ~3.5 Ar atoms. This separation in the photofragments begins with ~2 Ar atoms for the precursor $I_2^-\cdot Ar_{12}$ and increases to ~11.5 Ar atoms for $I_2^-\cdot Ar_{22}$, at which point it remains relatively constant. The two classes of m/e 254-based photofragments are illustrated in Fig. 6 for the precursor cluster sizes $n=13$ to 15. The separation between the two groups increases with precursor cluster size. For reasons explained in the discussion section, we refer to channel (d) photoproducts as ''sol-

vent separated'' and represent it as $(I^- \cdots I)$. Channel (c) photoproducts will be referred to as caged.

C. Laser fluence dependencies

The photofragment data for $n=13$ to 15 in Fig. 6 show two clearly separated m/e 254-based distributions. Such a bimodal distribution has not been observed in any of our previous caging studies and brings up the possibility of multiphoton processes. The laser used in these experiments has high peak power ($\sim$50 GW/cm^2); it may be possible to observe multiphoton absorption, even on a purely repulsive upper state surface. In particular, a two-photon absorption to the $^2\Pi_{u,1/2}$ state (Fig. 4) would result in the production of the spin orbit-excited state I* with $\sim$1 eV of trapped energy. In the absence of collisions, this state will not decay to the ground state on the τ_2 time scale. Such a process would result in the evaporation of fewer monomers since most of the photon energy would be trapped in the I*.

To address the possibility of multiphoton processes, the intensity of each distribution was measured as a function of laser fluence. The 790 nm power dependence study was carried out on $I_2^- \cdot Ar_{16}$ as follows. The laser was attenuated by using a series of neutral density filters, such that the attenuation ranged from zero to a factor of 15, corresponding to photon fluxes between 2.5×10^{15} and 0.17×10^{15} photons$\cdot$cm^{-2}. Each class of m/e 254-based photoproduct was refocused with the reflectron, and the intensity of both the fragments and the remaining precursor were integrated at various laser fluences. The signal was then normalized to the precursor ion intensity. This process was repeated five times in random order of laser attenuation. Even though the I_2^- absolute photoabsorption cross section at 790 nm is relatively large ($\sim2.5\times10^{-17}$ cm^2), there is still insufficient depletion ($<$10%) of the precursor ion, even at full laser power, to require a correction. The experimental data and resulting linear regression analysis for these distributions are shown in Fig. 7. Over the measured range, both plots are linear, demonstrating one-photon kinetics. Additionally, since all of the excited states are repulsive, the possibility of saturating a transition, and therefore making a multiphoton process appear as a one-photon process, is unlikely. Similar experiments have demonstrated that the observed uncaged photoproducts also arise from the absorption of one photon.

D. Cluster size dependence of photofragment distributions

To elucidate further the photophysics of I_2^- caging in Ar, the branching ratio, F_i, for each class of ionic photofragment was measured as a function of cluster size by using the following equation:

$$F_i = \frac{I(\mathrm{Pf}_i)}{\Sigma_i I(\mathrm{Pf}_i)}, \tag{6}$$

where $I(\mathrm{Pf}_i)$ is the integrated intensity of each class of photofragment (for a single cluster size), such that $\Sigma F_i = 1$. Although two sets of I^--based products are observable in the size range of $n=10$ to $n=14$, these sets are only completely resolvable for $n=13$ and $n=14$. Hence, in calculating the branching ratios, we group the two uncaged isomers together. The results are plotted in Fig. 8 and several features are immediately apparent. First, the uncaged, I^- photoproduct, channel closes at $n=17$. Second, there are no m/e 254-based photoproducts until $n=10$, at which point the relative intensity of both the $I_2^- \cdot Ar_m$ and $(I^- \cdots I) \cdot Ar_m$ channels increases rapidly as the precursor cluster size is increased, eventually leveling off at $n \geqslant 15$.

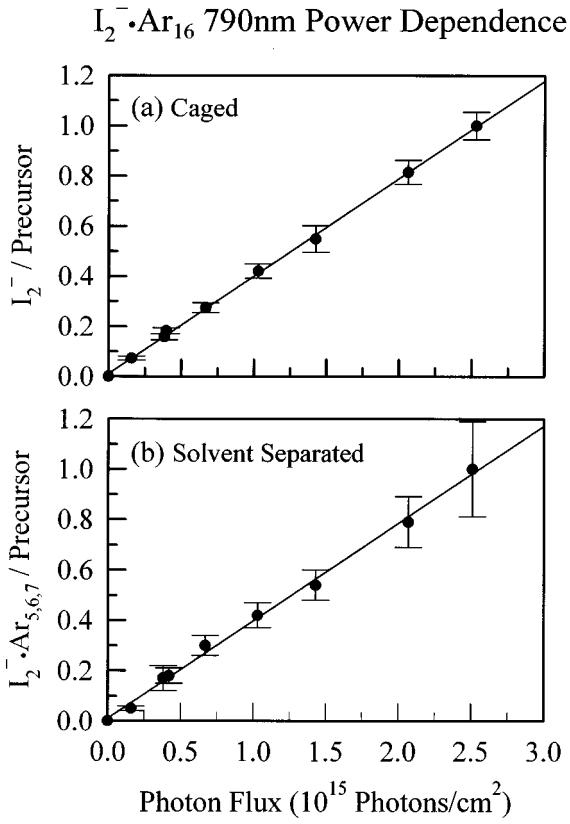

FIG. 7. Laser fluence dependence of both m/e 254-based distributions arising from the interaction of $I_2^- \cdot Ar_{16}$ with 790 nm laser light. Plot (a) shows the laser fluence dependence of the caged photoproduct (I_2^-) and the second plot (b) shows the dependence of the sum of the solvent separated photoproducts $[(I^- \cdots I) \cdot Ar_{5,6,7}]$.

VI. DISCUSSION

Before discussing the evaporation energetics, we comment on the distribution of $I_2^- \cdot Ar_n$ ions produced in the ion source and possible structural implications. As seen in Fig. 3, the mass spectrum exhibits intensity discontinuities at $n=13$, $n=20$, and $n=25$. Intensity discontinuities are usually attributed to increased stability for certain structures.[25,26] In our previous work[19] on $I_2^-(CO)_2$ clusters, a similar anomaly occurred at $n=16$ and was attributed to the completion of the first solvent shell around I_2^-. The intensity discontinuities in the mass spectra are, in part, caused by the shell closing of Ar around the I_2^-. However, without further information, we cannot determine exactly where the first solvation shell closes, and our best estimate is that it is in the range of 16 to 25 Ar atoms.

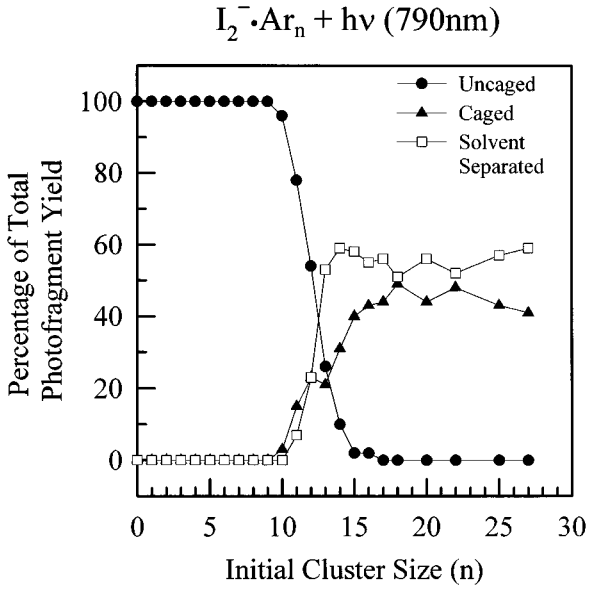

FIG. 8. Normalized branching ratios for the three distinct photoproduct channels (uncaged, caged, and solvent separated) at 790 nm, plotted as a function of cluster size. Cluster sizes that had two distributions of uncaged photofragments were averaged together.

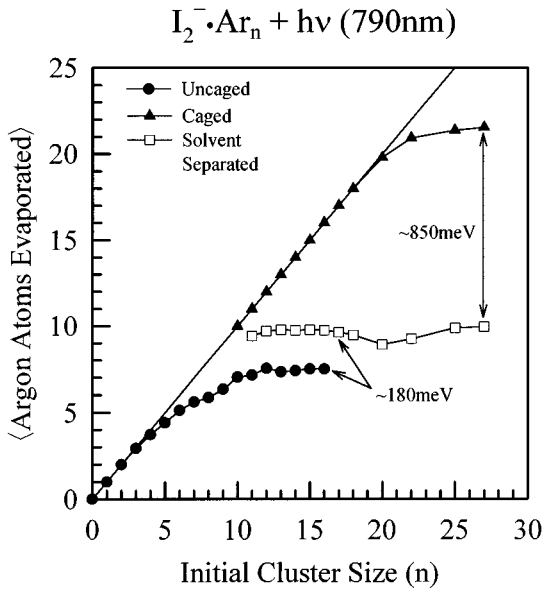

FIG. 9. Average number of Ar atoms evaporated for the uncaged, caged, and solvent separated product channels at 790 nm, plotted as a function of cluster size. The solid line represents the total number of Ar atoms in the precursor.

We will address several important issues concerning the results of this experiment. First, we discuss the evaporation energetics of the three types of photoproducts, uncaged, caged, and solvent separated. We then discuss the two m/e 254-based photoproduct channels, (c) and (d). A discussion on the origin of the two uncaged photoproducts, channels (a) and (b), follows. Finally, we compare the caging efficiency of I_2^- in Ar to that in CO_2.

A. Evaporation energetics of the three statistical photoproducts

An estimate of cluster binding energy can be extracted in the limit where the precursor ion is composed of a sufficient number of solvent molecules to dissipate, evaporatively, all the available photon energy. The average number of neutral atoms evaporated is calculated by

$$\text{Avg. evaporated} = \frac{\Sigma_a a I(a)}{\Sigma_a I(a)}, \tag{7}$$

where a is the number of Ar atoms evaporated for each fragment and $I(a)$ is the intensity of this channel. If this value is a constant as a function of cluster size, the binding energy can then be bounded above by Eq. (4), where the resulting value is the sum of the real binding energy and the kinetic energy release of evaporation. For large clusters the kinetic energy release is essentially thermal, and for the estimated temperature of 40 K, is ~5–10 meV per evaporation.[55] The kinetic energy release is expected to be larger for the earlier evaporations and decreases upon further loss of Ar atoms.

Photon energy is transferred to evaporation energy by two mechanisms. For uncaged photoproducts the dissociated I_2^- has not recombined, and only the kinetic energy release ($h\nu - D_0 = 0.45$ eV) is available for evaporation. For m/e 254-based photofragments, both the I^- and I remain in the cluster, and if the I_2^- bond is reformed, all of the photon energy is available for Ar evaporation. Evaporation then also proceeds via I_2^- vibrational energy transfer to the solvent translational modes. On the other hand, if the I_2^- bond is not reformed, only the kinetic energy release is available for Ar evaporation. In Fig. 9, the average number of neutral Ar atoms evaporated for each of the three types of photoproducts—uncaged, solvent separated, and caged—is plotted as a function of cluster size. Also shown is a solid line signifying the total number of Ar atoms in the precursor. In the large-cluster evaporation limit these three channels reach a constant evaporation of ~7.5, 9.9, and 21.5 Ar atoms, respectively. To estimate the Ar binding energy to the cluster, we use the average number of atoms evaporated in the caged and uncaged channels. The number of Ar atoms evaporated divided by the photon energy (1.57 eV) yields 73 meV binding energy per Ar atom for the caged asymptote. From the uncaged asymptote, a value of 67 meV is extracted. Note that the latter value was calculated by using 0.47 eV, the photon energy minus the dissociation energy. These values are comparable with earlier measurements on Ar_n^+ clusters[22] that placed a 90 meV upper bound to the binding energy of an Ar atom onto Ar_n^+. This somewhat larger value for the Ar_n^+ clusters presumably arises from the smaller ion core, allowing a closer approach of the Ar solvent to the positive charge.

The most striking observation in this study is the bimodal distribution of m/e 254-based photofragments. This bimodal behavior was not observed in previous $I_2^-(CO_2)_n$ experiments,[19] and its origin is not immediately obvious. We

know from mass analysis that all of these ions contain two I atoms. Comparison of the average number of Ar atoms evaporated shows that ~11.6 fewer Ar atoms are evaporated in this solvent-separated channel. Using 73 meV as the Ar binding energy, the energetic separation between the two groups is ~850 meV. Comparison to the uncaged curve yields a separation of ~180 meV. The total energetic separation (1.03 eV) between the caged and uncaged curves is comparable to the I_2^- bond energy of 1.1 eV.[64] The energetic location of the solvent-separated curve indicates that the ground-state I_2^- bond has not been reformed, even though both I atoms remain within the cluster. The likely origin of these ''solvent-separated'' clusters will be discussed in the next section.

The solvent-separated curve in Fig. 9 also shows a local minimum in the number of Ar atoms evaporated for $I_2^- \cdot Ar_{20}$. Here, the average number of atoms evaporated is about one monomer less than the neighboring clusters. This minimum indicates that this cluster has some additional stability, a result consistent with the local maximum at $I_2^- \cdot Ar_{20}$ in the precursor mass spectrum (Fig. 3). A study on benzene$^+$-Ar_n clusters[44] has also detected an intensity anomaly at $n=20$, but any relationship to these data is unclear.

B. Metastable unrecombined ($I^- \cdots I$) fragments

Photoproducts from the solvent-separated channel contain both I atoms within the cluster without reforming the ground-state I_2^- bond. Surprisingly, these metastable, fragment ions survive in a cluster of as few as two Ar atoms for at least 5 μs (τ_2). We cannot determine the structure of such a complex from the experimental data, but we can postulate two forms. These two I atoms exist either as separate atomic species ($I^- \cdots I$) or as an excited I_2^- state with an excitation energy of ~1 eV. The former will be discussed first.

1. Solvent-separated pair

Inspection of the asymptotes in Fig. 9 yields information on the role of the I atom as part of the solvent for the I^- moiety. The atomic I should be considered as a part of the solvent network, and it is interesting to estimate its binding energy. Examination of the asymptotes of the uncaged and solvent-separated fragment channels, from above, shows that they are separated by ~2.5 Ar atoms. When the dissociated I atom is not ejected from the cluster, it adds to the solvation of the I^- chromophore, and this extra release of energy is then available for evaporation of additional Ar atoms. This additional evaporation is the difference between the solvent-separated and uncaged curves in Fig. 9. The energetic separation between these two curves yields the binding energy of I to I^-. As calculated above, this is energy is ~180 meV, making the I atom ~2.5 times more ''sticky'' than an Ar atom. Interestingly, the difference in atomic polarizabilities between Ar and atomic I is a factor of 3, suggesting that in this case the solvent–solute interactions are largely governed by ion-induced dipole interactions, which scale linearly with polarizability.

In the limit of a small number of Ar solvent atoms, this energy arises primarily from the interaction between I^- and I. The potential-energy curves of Fig. 4 indicate a separation of ~5.5 Å for an energy 180 meV below the dissociation limit. The van der Waals radii of I and Ar are 2.15 and 1.90 Å, respectively, thus there could be room for an Ar atom between the two I atoms.

One possible configuration of the solvent separated pair is with the Ar atoms located symmetrically around the I^- with the other I on the ''outside'' of the cluster, thus preventing the two I atoms from coming into contact. Another possible structure would put the Ar atoms in the form of a ring around the waist of the $I^- \cdots I$ entity, keeping the two I atoms at a greater-than-equilibrium separation. In either case, the potential energy between I^- and I is dependent on the internuclear separation. Both configurations are metastable, since the I_2^- bond would be reformed in the global minimum-energy structure. For large clusters, this type of complex accounts for ~55% of the photoproducts.

2. Trapped excited state

Another possible structure for this photofragment is an I_2^- trapped on a slightly bound excited-state surface (e.g., the $^2\Pi_{g,3/2}$ state) at an energy ~180 meV below the (I^-+I) dissociation limit. For bare I_2^- the potential-energy curves in Fig. 4 indicate that the first excited state is bound by ~110 meV, whereas all the higher excited states are purely repulsive. If recombination occurs via a curve crossing to this state, it is possible that the I_2^- is trapped in this shallow well. The presence of a solvent could make the curve crossing facile. Although transient recombination into an excited state was observed[1] in the earlier studies of I_2^- in CO_2, there was no evidence for long-time trapping of I_2^- near the dissociation limit. Further, by using matrix absorption[66] and gas-phase data,[19] the radiative lifetime of the first excited state is estimated to be ~5 μs. Thus, there exists the possibility of recombination to the $^2\Pi_{g,3/2}$ state, followed by radiative decay to the ground state. In this case the ionic product would be an $I_2^- \cdot Ar_m$ cluster ion in its ground state.

However, given the similarities in time scales, this argument is only qualitative, and more experimental data are clearly necessary before the mechanism for formation of the evaporatively distinct isomers and their structure are understood. We have begun a series of pump-probe experiments on these clusters and expect that these experiments will further our understanding of this fragmentation process. In addition, molecular dynamics simulations that include excited-state surfaces are currently in progress by Parson and co-workers,[67] and the combination of experiment and theory should provide deeper insight into the origin of these unique fragments ions.

C. Isomeric forms of precursor $I_2^- \cdot Ar_n$ cluster ions

In addition to the two types of m/e 254-based photoproducts, two evaporatively distinct $I_2^- \cdot Ar_n$ isomers are formed in the ion source. This result can be observed via the fragment distributions of the uncaged photoproducts. The

uncaged photofragment distribution for $I_2^-\cdot Ar_{13}$ (Fig. 5) shows two groups of I^--based peaks, (a) and (b). The larger of the two has retained an average of 5.7 Ar atoms. Given the 68 meV binding energy of Ar onto I^- and the 470 meV energy available for evaporation, the average number of Ar atoms evaporated should be ~7.5, thus making the average number of retained Ar atoms ~5.5 for this cluster size. The consistency of these two numbers indicates that the products in this group came from precursors in which the I_2^- is embedded in the cluster's interior. The other group (a) retains an average of ~1 Ar atom. For these products to have come from a cluster with an interior solvated I_2^- implies that an additional 325 meV of energy had to be deposited into the cluster. Since no additional energy was deposited into the cluster, this fragment distribution must arise from clusters where the I_2^- resides on the surface rather than the interior. Additionally, the average number of Ar atoms retained in group (a) does not vary as a function of precursor cluster size, therefore further supporting the concept of a surface isomer. This isomer was only detected for $n=10-14$. For cluster sizes larger than $n=14$, this channel was not observed, therefore suggesting that in these clusters the ionic chromophore is embedded within the solvent. Such a metastable isomer is likely formed during the supersonic expansion by evaporation from larger clusters and becomes trapped in this configuration. This behavior was postulated theoretically[68] for the hydrated electron clusters, $(H_2O)_n^-$, where it was claimed there was an intermediate size regime in which the excess electron resided in a mixture of interior and surface locations. It has been suggested[14] that $I^-\cdot(H_2O)_n$ also exists, at least in part, with the ion residing on the surface; however, this argument rests on theoretical interpretation[69] and remains somewhat ambiguous. To our knowledge this is the first direct observation of different isomeric cluster ions in this size range.

D. Comparison of I_2^- caging in CO_2 and Ar at 790 nm

It is illustrative to characterize further the role of the solvent in the caging process by comparing the caging fractions of $I_2^-\cdot Ar_n$ to that of $I_2^-\cdot(CO_2)_n$ clusters at the same excitation energy. These data for 790 nm photoexcitation are plotted together in Fig. 10, where for Ar, only the recombined I_2^- fraction is plotted. It is apparent that the caging dynamics are quite different in these two solvents. Caging in CO_2 is first observed at $n=4$ and increases relatively monotonically until 100% caging is observed at $n=16$, the completion of the first solvation shell. The onset of caging in Ar begins at $n=10$ and reaches an asymptote of ~45% at about $n=16$.

Since CO_2 and Ar have approximately the same mass (44 and 40 amu) and thus similar solute–solvent kinematics, this pronounced difference in caging efficiency is attributable to the respective electrostatic properties: although CO_2 does not have a permanent dipole moment, its electric quadrupole moment is significant $(-4.3\times10^{-26}$ esu $cm^2)$[70] with an approximate charge distribution of minus one-half on each O atom and plus one on the C atom. This significant quadrupole moment has a strong effect on the packing of CO_2 around the I_2^- chromophore. In addition to stronger ion–solvent interactions in $I_2^-(CO_2)_n$ clusters, the CO_2–CO_2 interactions are stronger than the Ar–Ar interactions. Therefore, the CO_2 cage is expected to be much more rigid than the Ar cage. These results are consistent with the condensed-phase experiments in which higher caging efficiency is observed for neutral I_2 in more polar solvents.[71] It would be interesting to compare the caging efficiency of I_2^- in clusters with similar binding energies, but different partial charge distributions in order to investigate the effects of cluster structure on caging.

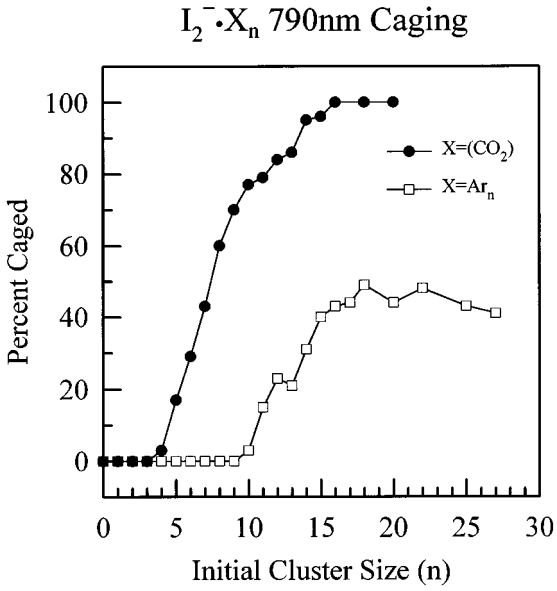

FIG. 10. A comparison of the caging efficiency of Ar and CO_2 as a function of cluster size.

Preliminary studies of I_2^- clustered in ammonia, water, and acetonitrile show significant caging at small cluster sizes, e.g., 10% with three ammonia monomers. These solvents have strong permanent dipole moments, and the $1/r^2$ ion–dipole interactions are longer range than the $1/r^3$ ion–quadrupole and $1/r^4$ ion–induced dipole interactions. The longer-range forces result in more efficient caging at smaller cluster sizes. Physically, this effect arises from polar solvent molecules being packed more rigidly around the I_2^-, thus creating a stronger cage. This stronger cage tends to keep the separating I atoms at relatively close internuclear separation and results in higher caging efficiency, even at small cluster sizes. However, one must be cautious in extending the interpretation of these results to larger cluster sizes and other solvents. For example, if the solvent–solvent interactions are stronger than the solute–solvent interactions, the solvent may begin clustering to itself as the cluster increases in size, leaving the solute on the outer surface of the cluster. This process would result in lower caging efficiency of the solute, a phenomenon not observed in solution where the solvent surrounds the solute.

VII. CONCLUSIONS

We have reported the caging dynamics of I_2^- in mass-selected Ar clusters in the size range from 1 to 27 Ar atoms and found four major evaporation processes. Two distinct isomers of the precursor ions were observed: (1) that of a normal interior solvated I_2^- and (2) that of an I_2^- residing on or near the surface of the Ar cluster. We also have observed a solvent separated $(I^- \cdots I)$ moiety in photofragments with as few as two Ar atoms. The photofragmentation distributions are compared with previous work on I_2^- in CO_2 clusters, and we suggest that the differences arise from the weaker electrostatic solute–solvent and solvent–solvent interactions in $I_2^- \cdot Ar_n$. Future work on I_2^- caging in other cluster solvents such as CS_2, N_2O, and others should shed further light on the importance of cluster structure on caging dynamics.

ACKNOWLEDGMENTS

We are pleased to acknowledge the helpful assistance of María E. Nadal and John M. Papanikolas and very stimulating conversations with Robert Parson, Paul E. Maslen, and James M. Faeder. We also gratefully acknowledge the support from the National Science Foundation under Grants No. CHE93-18639 and No. PHY90-12244. M.L. was supported by the JILA Visiting Fellow program.

[1] J. M. Papanikolas, V. Vorsa, M. E. Nadal, P. J. Campagnola, H. K. Buchenau, and W. C. Lineberger, J. Chem. Phys. **99**, 8733 (1993).
[2] L. Perera and F. G. Amar, J. Chem. Phys. **90**, 7354 (1989).
[3] P. E. Maslen, J. M. Papanikolas, J. Faeder, R. Parson, and S. V. Oneil, J. Chem. Phys. **101**, 5731 (1994).
[4] Q. L. Liu, J. K. Wang, and A. H. Zewail, J. Phys. Chem. **0099**, 11 321 (1995).
[5] J. K. Wang, Q. L. Liu, and A. H. Zewail, J. Phys. Chem. **0099**, 11 309 (1995).
[6] Q. Liu, J.-K. Wang, and A. H. Zewail, Nature **364**, 427 (1993).
[7] E. D. Potter, Q. Liu, and A. H. Zewail, Chem. Phys. Lett. **200**, 605 (1992).
[8] S. Fei, X. Zheng, M. C. Heaven, and J. Tellinghuisen, J. Chem. Phys. **97**, 6057 (1992).
[9] X. Hu and C. C. Martens, J. Chem. Phys. **99**, 9532 (1993).
[10] D. W. Boo and Y. T. Lee, J. Chem. Phys. **103**, 520 (1995).
[11] T. J. Selegue, N. Moe, J. A. Draves, and J. M. Lisy, J. Chem. Phys. **96**, 7268 (1992).
[12] S. G. Donnelly and J. M. Farrar, J. Chem. Phys. **98**, 5450 (1993).
[13] D. J. Lavrich, D. Serxner, M. A. Buntine, and M. A. Johnson, J. Chem. Phys. (in press).
[14] G. Markovich, S. Pollack, R. Giniger, and O. Cheshnovsky, J. Chem. Phys. **101**, 9344 (1994).
[15] D. W. Arnold, S. E. Bradforth, E. H. Kim, and D. M. Neumark, J. Chem. Phys. **97**, 9468 (1992).
[16] D. W. Arnold, S. E. Bradforth, E. H. Kim, and D. M. Neumark, J. Chem. Phys. **102**, 3493 (1995).
[17] L. N. Ding, P. D. Kleiber, M. A. Young, Y. C. Cheng, S. V. ONeil, and W. C. Stwalley, J. Chem. Phys. **102**, 5253 (1995).
[18] S. T. Arnold, J. H. Hendricks, and K. H. Bowen, J. Chem. Phys. **102**, 39 (1995).
[19] J. M. Papanikolas, J. R. Gord, N. E. Levinger, D. Ray, V. Vorsa, and W. C. Lineberger, J. Phys. Chem. **95**, 8028 (1991).
[20] H. Haberland, in *Clusters of Atoms and Molecules; Theory, Experiment, and Clusters of Atoms*, edited by H. Haberland (Springer-Verlag, Berlin, 1994), Vol. 52, pp. 374–395.
[21] H. Haberland, B. v. Issendorf, T. Kolar, H. Kornmeier, C. Ludewigt, and A. Risch, Phys. Rev. Lett. **67**, 3290 (1991).
[22] N. E. Levinger, D. Ray, M. L. Alexander, and W. C. Lineberger, J. Chem. Phys. **89**, 5654 (1988).
[23] K. Hiraoka and T. Mori, J. Chem. Phys. **90**, 7143 (1989).
[24] T. Nagata and T. Kondow, J. Chem. Phys. **98**, 290 (1993).
[25] T. D. Mark, P. Scheier, K. Leiter, W. Ritter, K. Stephan, and A. Stamatovic, Int. J. Mass Spectrosc. Ion Proc. **74**, 281 (1986).
[26] I. A. Harris, R. S. Kidwell, and J. A. Northby, Phys. Rev. Lett. **53**, 2390 (1984).
[27] M. Foltin, G. Walder, S. Mohr, P. Scheier, A. W. Castleman, Jr., and T. D. Märk, Z. Phys. D **20**, 157 (1991).
[28] M. Foltin, G. Walder, A. W. Castleman, Jr., and T. D. Märk, J. Chem. Phys. **94**, 810 (1991).
[29] D. Barton Smith and J. C. Miller, J. Chem. Phys. **90**, 5203 (1989).
[30] W. Miehle, O. Kandler, T. Leisner, and O. Echt, J. Chem. Phys. **91**, 5940 (1989).
[31] H. Steger, J. d. Vries, W. Kamke, and I. V. Hertel, Z. Phys. D **21**, 85 (1991).
[32] G. Ganteför, G. Broker, E. Holub-Krappe, and A. Ding, J. Chem. Phys. **91**, 7972 (1989).
[33] J. A. Smith, N. G. Gotts, J. F. Winkel, R. Hallett, C. A. Woodward, A. J. Stace, and B. J. Whitaker, J. Chem. Phys. **97**, 397 (1992).
[34] J. J. Sáenz, J. N. Soler, and N. Garciá, Chem. Phys. Lett. **114**, 15 (1985).
[35] H.-U. Böhmer and S. D. Peyerimhoff, Z. Phys. D **11**, 239 (1989).
[36] P. J. Kuntz and J. Valdorf, Z. Phys. D **8**, 195 (1988).
[37] N. E. Levinger, D. Ray, K. K. Murray, A. S. Mullin, C. P. Schulz, and W. C. Lineberger, J. Chem. Phys. **89**, 71 (1988).
[38] M. J. DeLuca and M. A. Johnson, Chem. Phys. Lett. **162**, 445 (1989).
[39] T. F. Magnera and J. Michl, Chem. Phys. Lett. **192**, 99 (1992).
[40] J. T. Snodgrass, C. M. Roehl, and M. T. Bowers, Chem. Phys. Lett. **159**, 10 (1989).
[41] F. X. Gadea and M. Amarouche, Chem. Phys. **140**, 385 (1990).
[42] A. J. Stace and D. M. Bernard, Chem. Phys. Lett. **146**, 531 (1988).
[43] Y. Zhao, I. Yourshaw, C. C. Arnold, and D. M. Neumark, J. Chem. Phys. **101**, 6538 (1994).
[44] C. Guillaume, J. L. Calve, I. Dimicoli, and M. Mons, Z. Phys. D **32**, 157 (1994).
[45] E. J. Bieske, A. M. Soliva, A. Friedmann, and J. P. Maier, J. Chem. Phys. **96**, 7535 (1992).
[46] R. L. Asher, D. A. Micha, and P. J. Brucat, J. Chem. Phys. **96**, 7683 (1992).
[47] P. Jungwirth and R. B. Gerber, J. Chem. Phys. **102**, 8855 (1995).
[48] T. D. Mark and P. Scheier, J. Chem. Phys. **87**, 1456 (1987).
[49] S. Wei, Z. Shi, and A. W. Castleman, J. Chem. Phys. **94**, 8604 (1991).
[50] D. Kreisle, O. Echt, M. Knapp, and E. Recknagel, Phys. Rev. A **33**, 768 (1986).
[51] M. Amararouche, G. Durand, and J. P. Malrieu, J. Chem. Phys. **88**, 1010 (1988).
[52] C. E. Klots, J. Chem. Phys. **83**, 5854 (1985).
[53] C. E. Klots, Z. Phys. D **20**, 105 (1991).
[54] P. C. Engelking, J. Chem. Phys. **85**, 3103 (1986).
[55] P. C. Engelking, J. Chem. Phys. **87**, 936 (1987).
[56] P. J. Campagnola, L. A. Posey, and M. A. Johnson, J. Chem. Phys. **95**, 7998 (1991).
[57] C. Brechignac, P. Cahuzac, and F. Carlier, J. Chem. Phys. **88**, 3022 (1982).
[58] M. L. Alexander, M. A. Johnson, and W. C. Lineberger, J. Chem. Phys. **82**, 5288 (1985).
[59] M. L. Alexander, M. A. Johnson, N. E. Levinger, and W. C. Lineberger, Phys. Rev. Lett. **57**, 976 (1986).
[60] S. Wei, W. B. Tzeng, and A. W. Castleman, Jr., J. Chem. Phys. **92**, 332 (1990).
[61] M. A. Johnson and W. C. Lineberger, in *Techniques for the Study of Ion Molecule Reactions*, edited by J. M. Farrar and J. W. Saunders (Wiley, New York, 1988), pp. 591–635.
[62] M. L. Alexander, N. E. Levinger, M. A. Johnson, D. Ray, and W. C. Lineberger, J. Chem. Phys. **88**, 6200 (1988).
[63] E. C. M. Chen and W. E. J. Wentworth, J. Phys. Chem. **89**, 4099 (1985).
[64] M. E. Nadal, J. M. Faeder, P. Kleiber, and W. C. Lineberger (in preparation).
[65] W. C. Lineberger, M. E. Nadal, P. J. Campagnola, V. Vorsa, P. D. Kleiber, J. M. Papanikolas, P. E. Maslen, J. Faeder, R. Parson, and O. Poplawski, in *Proceedings of the Robert A. Welch Foundation 38th Conference on Chemical Research: Chemical Dynamics of Transient Species* (R. A. Welch Foundation, Houston, TX, 1994), Vol. 38, pp. 175–184.
[66] C. J. Delbecq, W. Hayes, and P. H. Yuster, Phys. Rev. **121**, 1043 (1961).

[67] P. E. Maslen, J. M. Faeder, and R. Parson (in preparation).
[68] R. N. Barnett, U. Landman, C. L. Cleveland, and J. Jortner, Chem. Phys. Lett. **145**, 382 (1988).
[69] L. Perera and M. L. Berkowitz, J. Chem. Phys. **96**, 8288 (1992).
[70] M. R. Battaglia, A. D. Buckingham, D. Neumark, R. K. Pierens, and J. H. Williams, Mol. Phys. **43**, 1015 (1981).
[71] A. L. Harris, J. K. Brown, and C. B. Harris, Annu. Rev. Phys. Chem. **39**, 341 (1988).